Journal of Biomedical Optics

SPIEDigitalLibrary.org/jbo

Optical coherence tomography platform for microvascular imaging and quantification: initial experience in late oral radiation toxicity patients

Bahar Davoudi
Melanie Morrison
Kostadinka Bizheva
Victor X. D. Yang
Robert Dinniwell
Wilfred Levin
I. Alex Vitkin

SPIE

Optical coherence tomography platform for microvascular imaging and quantification: initial experience in late oral radiation toxicity patients

Bahar Davoudi,[a] Melanie Morrison,[a] Kostadinka Bizheva,[b] Victor X. D. Yang,[c] Robert Dinniwell,[d,e] Wilfred Levin,[d,e] and I. Alex Vitkin[a,d,e]
[a]University of Toronto, Department of Medical Biophysics, Toronto, Ontario M5G 2M9, Canada
[b]University of Waterloo, Department of Physics and Astronomy, Waterloo, Ontario N2L 3G1, Canada
[c]Ryerson University, Department of Electrical and Computer Engineering, Toronto, Ontario M5B 2K3, Canada
[d]University Health Network, Ontario Cancer Institute, Toronto, Ontario M5G 2M9, Canada
[e]University of Toronto, Department of Radiation Oncology, Toronto, Ontario M5S 3S2, Canada

Abstract. An optical coherence tomography (OCT) microvascular imaging platform, consisting of Doppler (DOCT) and speckle variance (svOCT) modalities, and microvascular image quantification tools are developed. The quantification methods extract blood flow-related parameters from DOCT images and vessel morphological parameters from svOCT images. This platform is used to assess the microvascular (DOCT and svOCT) images obtained during a clinical study on late oral radiation toxicity. This specific pathology was considered a suitable scenario for verifying the performance of the developed quantification platform because late oral radiation toxicity is known to involve microvascular damage. The derived parameters are compared between several DOCT and svOCT images from one patient and one healthy volunteer as proof-of-principle, and the significance of the observed differences is discussed. Given the low number of OCT clinical studies that measure and quantify microvascular images and considering the importance of such quantification in a number of pathologies, this newly developed platform can serve as a useful tool in studying diseases and treatments with microvascular involvement. [DOI: 10.1117/1.JBO.18.7.076008]

Keywords: optical coherence tomography; microvascular imaging; image quantification; late oral radiation toxicity; Doppler optical coherence tomography; speckle variance optical coherence tomography.

Paper 130121R received Mar. 4, 2013; revised manuscript received May 24, 2013; accepted for publication Jun. 4, 2013; published online Jul. 10, 2013.

1 Introduction

Optical coherence tomography (OCT) is a micron-scale-resolution imaging modality that can capture subsurface structural images within 1 to 2 mm below the surface of most biological tissues.[1] Since its emergence in the 1990s,[2] it has been actively researched by the biophotonics and medical imaging communities,[3–5] with significant technological advances in various preclinical and clinical studies.[5,6] OCT images of tissue microstructure can be supplemented by those of microvasculature[7,8] to add important physiological and functional information to clinical imaging. Among the OCT microvascular imaging methods, Doppler OCT (DOCT) has captured a lot of attention due to its ability to provide information on blood velocity as slow as tens of micrometers per second.[9,10] Moreover, speckle variance OCT (svOCT)[11] is another OCT-based microvascular imaging technique that can visualize microvessels as small as tens of micrometers in diameter.[11]

While microvascular OCT imaging is of interest due to the additional functional information it provides, it is not often performed in clinical studies because of technological challenges, including system issues such as phase noise, or challenges associated with tissue motion.[9,11] For example, among the ~400 registered clinical trials which use OCT,[12] only about 2.5% involve some vascular OCT measurements. Furthermore, quantification of the acquired microvascular OCT images is often lacking. Yet, image quantification and extraction of numerical metrics to provide precise information on the changes in microvascular features are essential for clinical decision making in vascular pathology cases, such as telangiectasia and hemangioma.[13,14]

We have recently built an OCT system for imaging human oral microvasculature *in vivo* through acquiring DOCT and svOCT images. Furthermore, we have developed a quantification tool to extract certain metrics from the acquired DOCT and svOCT images as an objective method to assess the microvascular abnormalities in oral pathologies. To verify that the developed quantitative metrics were able to highlight the differences between pathological and healthy cases, we analyzed the microvascular images acquired during our recently initiated clinical study on late oral radiation toxicity patients. Late oral radiation toxicity occurs in ~50% of the head and neck cancer patients who undergo radiation therapy.[15] These late effects are mainly caused by damage to the microvasculature of the oral tissue and manifest as morphological or blood flow-related changes in the vessels, such as changes in vessel size and diameter, vessel architecture, and average blood velocity.[13,16] Therefore, this clinical problem served as a representative case of microvascular pathology where the developed OCT microvascular image quantification method could be tested. To the best of

Address all correspondence to: Bahar Davoudi, University of Toronto, Department of Medical Biophysics, Toronto, Ontario, Canada. Tel: 001 416 946 4501; E-mail: bahar.davoudi@utoronto.ca

our knowledge, this is the first time a DOCT and svOCT microvascular image quantification platform has been developed to address this important clinical problem.

In this article, the developed vascular quantification metrics are introduced and their calculation methods from DOCT and svOCT images are explained. As proof of principle, the results of calculating these metrics in up to 20 microvessels of one late oral radiation toxicity patient and one healthy volunteer from the ongoing clinical study are presented.

2 Methods

2.1 *OCT Oral Imaging*

A spectral domain OCT system was designed and built for acquiring microstructural and microvascular OCT images [Fig. 1(a)]. The light source consisted of two superluminescent diodes (Superlum Ltd., Carrigtwohill, County Cork, Ireland) with a combined broad emission bandwidth of 113 nm centered at 1322 nm, with an output power of 13 mW.[17] A spectrometer and a linear array charge-coupled device (CCD) camera (Goodrich Corp., Charlotte, North Carolina, 1024 pixels) were used for signal detection.[17] The axial resolution and the penetration depth of the system in tissue were ~5.1 μm and ~1.4 mm, respectively. The high A-scan rate of the system (47 kHz) along with the fast moving galvanometers enabled acquisition of real-time two-dimensional (2-D) structural B-mode images and three-dimensional (3-D) DOCT and svOCT data sets.

An OCT imaging probe was designed and built specifically for oral imaging [Fig. 1(b)]. The probe consisted of a hollow rigid tube of 2 cm outer diameter which housed three lenses. This relay configuration focused the collimated incident light from the OCT fiber network onto the tissue and picked up retro-reflected light.[17] The probe was attached to a housing unit containing galvanometers for beam scanning. To make patient-specific adjustments to probe and galvo box configuration during the clinical imaging sessions, a translation stage providing 3 degree of freedom and a rotation stage providing 6 degree of freedom were used. The imaging system and the oral OCT probe were integrated onto a portable cart and were approved by the Canadian Standard Association for hospital use. A clear 200-μm thick glass cover was glued to the distal end of the probe to facilitate disinfection between consecutive patient imaging sessions. The probe was also wrapped in a sterilized disposable transparent sheath.

During clinical imaging, the patient or the healthy volunteer sat on a chair in front of the OCT probe and placed their chin and forehead on the chin rest and forehead rest [Fig. 1(c)] and kept their mouth open. The probe was then inserted into their mouth for imaging.[17] An average of 10 to 15 3-D data sets were acquired from each subject in this study. 3-D sets of svOCT images consisted of ~200 and 3-D datasets of DOCT consisted of ~100 2-D B-scans (1 mm lateral × 1.1 mm depth). These data sets were acquired from both oral regions with visible complications and regions devoid of any complications. Acquiring each 3-D data set took ~7 s. After each clinical session, the data was processed to form corresponding DOCT and svOCT 3-D images.

2.2 *Clinical Study*

Late oral radiation toxicity patients at Princess Margaret Hospital (Toronto, Canada) were invited to participate in this OCT feasibility study; individuals with no sign of oral disorder were also approached to participate as healthy volunteers. Written consent was acquired from all. The study was approved by the Research Ethics Board for 15 patients and 5 healthy volunteers. In this article, interim preliminary results from one healthy volunteer and one patient are presented. Human imaging was performed in compliance with the relevant laws and institutional guidelines in accordance with the ethical standards of the Declaration of Helsinki.[18]

2.3 *DOCT Image Quantification*

DOCT is a method of blood velocity measurement. It essentially detects the velocity component of red blood cells parallel to the incident laser beam, based on the classical Doppler effect.[9,10] To form DOCT images, phase shift values were calculated over consecutive depth scans (A-scans) using Kasai estimator.[9,17] The phase shift was then converted to axial velocity via $V_z = \lambda_0 \cdot \Delta\Phi/4\pi n \cdot \Delta t$,[17] where V_z is the red blood cell velocity along the beam direction, λ_0 is the central wavelength of the light source, $\Delta\Phi$ is the measured average phase shift over the vessel cross-section, n is the tissue refractive index, and Δt is the time between consecutive phase measurements. To extract the velocity vector from the axial velocity component, the angle between incident beam and vessel axis (Doppler angle) had to be determined through analyzing the 3-D DOCT data sets.

To calculate the first DOCT-based quantification metric (average velocity V), the axial velocity component (V_z) was

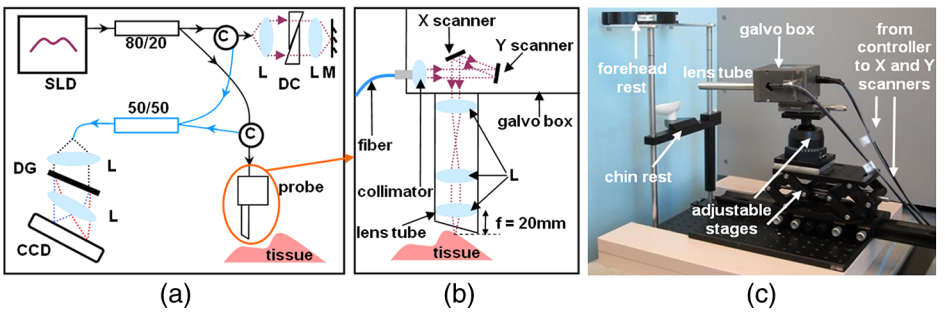

Fig. 1 (a) Schematic of the spectral domain OCT system: SLD: superluminescent diode, C: circulator, L: lens, DC: dispersion compensation unit, M: mirror, DG: diffraction grating. Using an 80/20 coupler at the input and a 50/50 one at the output enabled transmission of maximum power to the sample arm while keeping the reference arm power below the CCD saturation level. (b) Schematic of the probe's optical design. The light is coupled from the fiber to free space and is focused on the tissue at a working distance of $f = 20$ mm from the objective lens. (c) Photograph of the oral OCT imaging probe attached to adjustable stages. The head frame (consisting of a forehead and a chin rest) helps to stabilize the subject's head during imaging.

divided by cos θ, where θ was the measured angle between the incident beam and the vessel axis. The flowchart of DOCT image formation and quantification is presented in Fig. 2(a), with the vessel boundary selection and Doppler angle demonstrated in Fig. 2(b).

The second quantification metric that was calculated based on DOCT images was pulsatility index (PI). This metric is a physiologically important measure of the difference between systolic and diastolic pressures, previously used as an indicator of peripheral vascular resistance in ultrasound studies.[19] It was calculated from $(V_{max} - V_{min})/V_{avg}$, where V_{max} is the maximum velocity (measured on the DOCT B-mode image which showed the maximum velocity in the vessel of interest, representing the systole), V_{min} is the minimum velocity (measured on the DOCT B-scan which showed the minimum velocity in the vessel of interest, representing the diastole), and V_{avg} is the average velocity in the vessel of interest over all the DOCT B-scans where the vessel was present.

In order to compare the two developed metrics for the microvessels of the same diameter range between the patient and the healthy volunteer, mean microvessel diameters were calculated from the DOCT images. Two-dimensional cross-sections of the 3-D DOCT images were examined in different orthogonal planes so that a circular, lateral, or elliptical cross-sectional view of the vessel could be obtained. Figure 3(c) demonstrates the diameter measurement method for the cases where a circular or lateral vessel cross-section was visible. For the elliptical cross-sections, however, the geometrical mean (square root of the product) of major and minor axes was taken [Fig. 3(d)]. We note that the DOCT vessel diameter analysis was not accurate enough to qualify as a legitimate metric in the developed platform, so it was only used for categorizing microvessels into similar size ranges for the described average velocity and PI calculations. Based on these measurements, microvessels were categorized into three groups based on their diameter, d: (1) $d < 50$ μm, (2) 50 μm $< d <$ 100 μm, and (3) 100 μm $< d <$ 150 μm. Since the number of vessels in the second and third groups were low (two in both the patient and the healthy volunteer), the subsequent blood flow quantification was only performed on the vessels of the first group.

Other potential DOCT microvascular metrics could be derived[10] but were not pursued in this feasibility study because (1) resolution limitation, phase noise and motion artifacts in this challenging *in vivo* imaging scenario inhibited visualization of the capillary network $\sim <$ 15 μm in diameter, (2) the svOCT microvascular data set (Sec. 2.4) allowed better visualization and more detailed analysis of vessel morphological features.

2.4 *SvOCT Imaging and Quantification*

SvOCT provides a microvascular map which, unlike Doppler, is independent of the Doppler angle of flow velocity. This

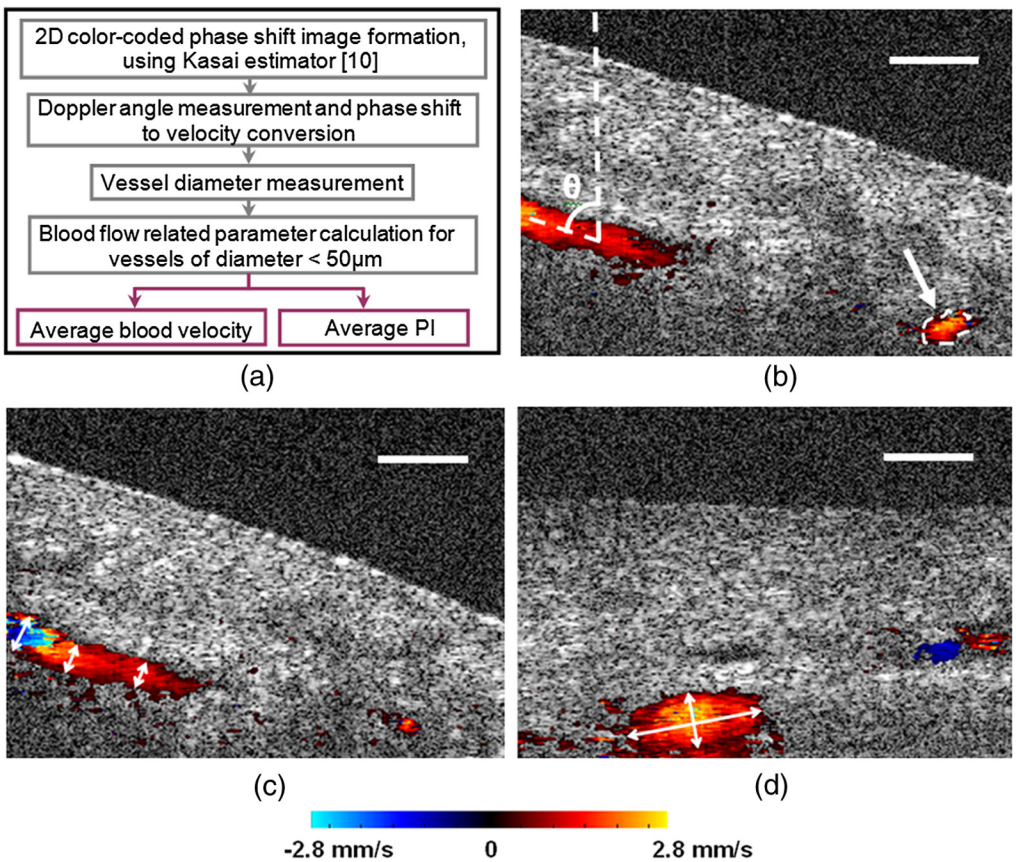

Fig. 2 (a) Summary of the steps taken for DOCT image quantification. (b)–(d) DOCT signals overlaid on the structural OCT images from the oral radiation toxicity patient, demonstrating the methods for finding Doppler-related blood flow parameters. (b) Example of Doppler angle calculation (vessel on the left) and region of interest selection (vessel on the right) within which the average blood velocity was calculated. (c) Example of vessel diameter calculation based on a lateral cross-section: diameter at three locations was measured and averaged to yield the average vessel diameter. (d) Example of vessel diameter calculation when the vessel cross-section was elliptical: the major and minor diameters of the ellipse were measured and their geometrical mean was defined as the diameter. Scale bars = 200 μm.

microvascular imaging technique relies on the temporal variance of the OCT structural speckle pattern that differs between bulk (solid) tissue and blood vessel (fluid) regions.[11] To form svOCT images, several B-scans taken at the same location were analyzed for temporal texture stability,[17] pixel by pixel. The temporal speckle variance over these B-scans was then calculated for each pixel in the 2-D slice:[20]

$$\mathrm{SV}_{ijk} = \frac{1}{N}\sum_{n=1}^{N}\left(I_{ijkn} - \frac{1}{N}\sum_{n=1}^{N} I_{ijkn}\right)^2, \qquad (1)$$

where SV_{ijk} is the speckle variance signal for the pixel of coordinates i, j, and k, I_{ijk} is the intensity of the same pixel, and N is the total number of B-scans over which the variance calculation was performed ($N = 4$ in this study).

Afterward, all of the 2-D slices were aligned to form a 3-D volume. Each pixel in the formed 3-D volume shows the value of speckle variance for that particular tissue voxel. Regions of higher temporal variance correspond to blood vessels (due to faster motion in lower viscosity "fluid," thus faster decorrelation) and regions of low variance correspond to bulk "solid" tissue.[11,17] The flowchart of svOCT image formation and quantification is presented in Fig. 3(a).

The first step to extract the microvascular morphology parameters was segmenting the vessels to separate them from the noisy or streaky artifactual regions because involuntary head motion caused image artifacts such as horizontal streaks in the svOCT images[11] [Fig. 3(b)]. Since the number of vessels present in a typical cubic millimeter of imaged tissue was relatively low (~6 to 13), partial manual segmentation was performed on the 3-D noisy svOCT images using Simple Neurite Tracer plug-in in ImageJ.[21,22] The traces were drawn manually along the center of the vessels and 3-D vessel filling was performed automatically around these traces [Fig. 3(d) and 3(e)]. The filling process was

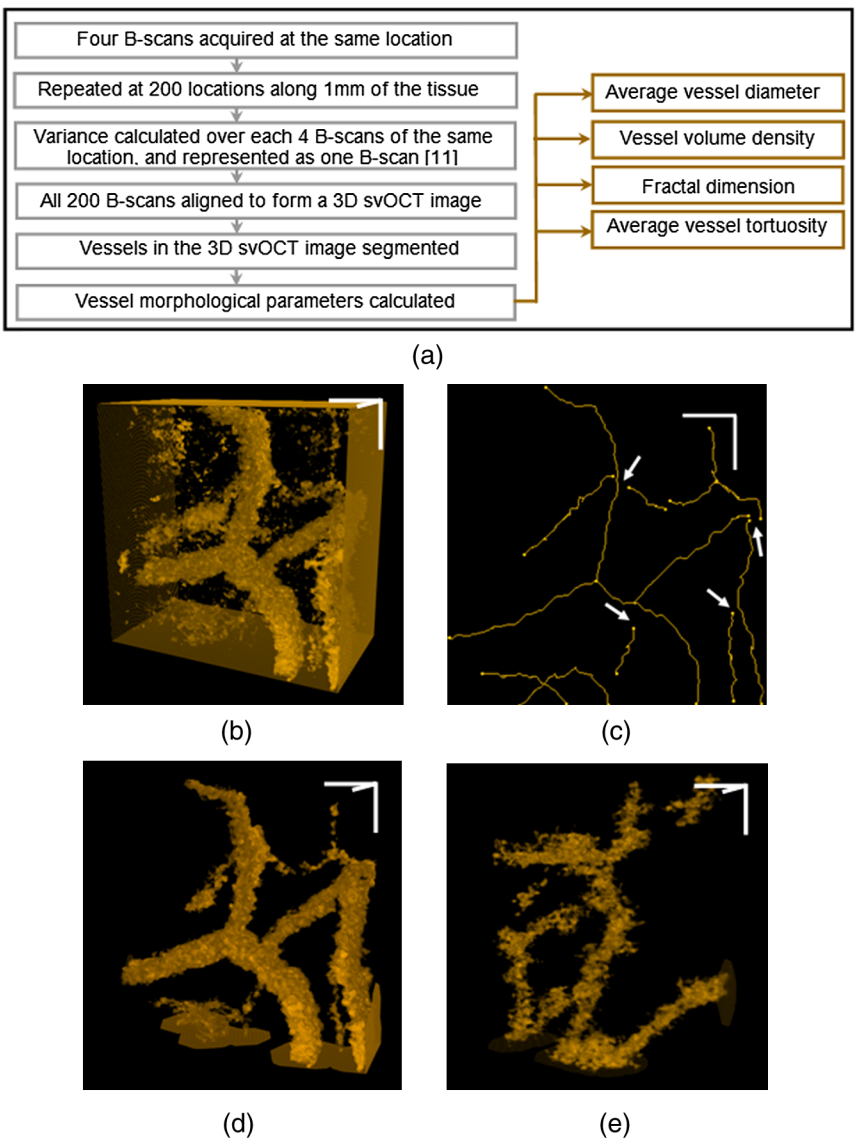

Fig. 3 (a) Summary of the steps taken for svOCT image construction and quantification. (b) 3-D representation of the raw (noisy) svOCT image calculated from the structural OCT images of a healthy volunteer. (c) The traces drawn along the center of the vessels in (b). The discontinuity between some branched vessels and their main branch (shown with white arrows) was because the traces were drawn along the vessel center while the branched vessels started from the outer surface of the main branch vessel. (d) Segmented vessels shown in (b) after the traces in (c) were automatically filled out [compare with (b)]. (e) 3-D representation of svOCT segmented vessels in a radiation toxicity patient. Scale bars = 200 μm.

stopped by the user upon reaching the boundaries of the vessel. The quantification parameters were then extracted from these segmented 3-D svOCT vasculature maps, as described below.

The first derived metric based on the svOCT images was an average microvessel diameter. A distance measurement tool in Simple Neurite Tracer[22] was used to measure this parameter for each of the segmented vessels at two or three different locations (based on the vessel length). Elliptical vessel cross-sections were handled similarly to the DOCT analysis described in Sec. 2.3. The average of each set of measurements was taken as the diameter for that vessel. The same was performed for all the vessels in each svOCT image, and the average of all these measurements was taken as the average vessel diameter in that image.

The second calculated parameter was the average blood vessel volume density. Simple Neurite Tracer[22] was used to calculate the total number of svOCT-positive vessel pixels and the total number of pixels in the 3-D volumes, with the ratio yielding an estimate of the blood vessel volume density. For each 3-D svOCT image ($\sim 1\ \text{mm} \times 1\ \text{mm} \times 500\ \mu\text{m}$), four vessel volume density measurements were performed over boxes of $\sim 750 \times 750 \times 500\ \mu\text{m}^3$, fitted to four corners of the image. The average of these four measurements was reported as the average vessel volume density. Calculating vessel density from 2-D histology slides has been used as a gold standard to assess vascular changes in pathology cases.[23–25] The potential advantages of this svOCT metric over the histological ones are its *in vivo* capability, avoidance of biopsies and tissue staining, and volumetric versus 2-D information content.

The third svOCT-based metric was fractal dimension (FD) of the vascular tree. This parameter is a measure of microvessel network self-similarity at different spatial scales and has previously been used as a measure of "well regulated" (~normal) or "chaotic" (~tumor) vasculature.[26,27] Higher FD has been found to indicate a more normal vascular and capillary network, better extended throughout the tissue.[26] This parameter has also been correlated to how "twisty" and "bendy" the vessels are.[26] As such, FD may report if radiation toxicity resulted in formation of tortuous vessels. In this study, this parameter (FD) may also correlate with radiation-induced vascular disorganization, leading to neovascularization which may be less space-filling compared with healthy vessels. To our knowledge, this is the first time that FD was being used to characterize the difference between radiation damaged and healthy microvasculature; our aim was thus to test if this metric can characterize such changes. To calculate FD, a fixed box counting method in FracLac (an ImageJ plug-in)[21,28] was used. Same as the vessel volume density calculation, FD was measured over four boxes of $\sim 750 \times 750 \times 500\ \mu\text{m}^3$, fitted to four corners of the image, and the average of these four measurements was reported as the average FD.

The final svOCT-based calculated metric was vessel tortuosity. This parameter was calculated manually using an algorithm described previously,[29] where tortuosity is defined as the ratio between the actual length of a vessel and the Euclidean distance between its two endpoints multiplied by a curvature indicator scalar. This scalar is equal to one plus the number of times the vessel of interest changed its curvature along the field-of-view.

Paired Student's *t*-test[30] was performed on the six calculated parameters (two DOCT and four svOCT) and was compared between the patient and the healthy volunteer, as a measure of the statistical significance of the observed differences between the two cohorts.

3 Results

The developed microvascular imaging and quantification platform were used in our ongoing clinical feasibility study. The developed metrics were extracted from DOCT and svOCT images acquired from one late oral radiation toxicity patient and one healthy volunteer. Initial comparison between these metrics is demonstrated in this section.

3.1 *DOCT-Based Blood Flow-Related Parameters*

Figure 4(a) demonstrates that the average blood velocity over all imaged oral regions in the radiation toxicity patient was about 1.8 times higher compared to the healthy volunteer. The p-value of this comparison shows a statistically significant difference between the two cohorts. The number of available microvessels with $d < 50\ \mu\text{m}$ for this measurement was ~20 vessels in the patient and ~10 in the healthy volunteer.

In order to calculate the PI, the microvessel had to be monitored during a few heart cycles, so that minimum and maximum velocity values (corresponding to diastole and systole, respectively) could be found. Therefore, we performed this calculation only on the microvessels present in DOCT images through a few heart cycles (approximately six vessels for each cohort). The resulting average PI over all imaged oral regions in the patient shows a two-fold increase compared to the healthy volunteer [Fig. 4(b)]. The p-value of this comparison is close to the common significance threshold ($p = 0.05$).

We also used the developed quantification platform to verify how average blood velocity and PI were different in specific oral regions of the same patient which received different radiation doses. Therefore, these two parameters were calculated and compared between the soft palate of: (1) the healthy volunteer; (2) the patient which received lower radiation (~47 to 53 Gy), known as the contralateral side, and (3) the same patient corresponding to the tumor site, which received ~56 to 66 Gy of radiation (so-called ipsilateral side). The results in Fig. 4(c) and 4(d) demonstrates an increase in the average values of blood velocity and PI in the soft palate with increased radiation dose.

3.2 *SvOCT-Based Morphological Vascular Parameters*

A total of 8 vessels in the patient's and 13 in volunteer's labial (lip mucosa) svOCT images were used to calculate the vessel morphology quantification parameters.

Figure 5(a) shows a greater presence of finer vessels in the irradiated tumor site (patient) compared to the healthy volunteer; however, the p-value does not represent a significant difference between the two. Figure 5(b) shows that the volume density of microvasculature in the healthy volunteer is considerably higher (~3×) compared to the patient case. The p-value for this comparison suggests a statistically significant reduction in microvasculature with irradiation. As per Fig. 5(c) and 5(d), the vessel FD and tortuosity metrics do not reveal statistically significant differences between the healthy and irradiated tissue, at least in this preliminary examination of one patient and one healthy volunteer.

4 Discussion

OCT microvascular imaging techniques, specifically DOCT and svOCT, have shown promise for *in vivo* monitoring of

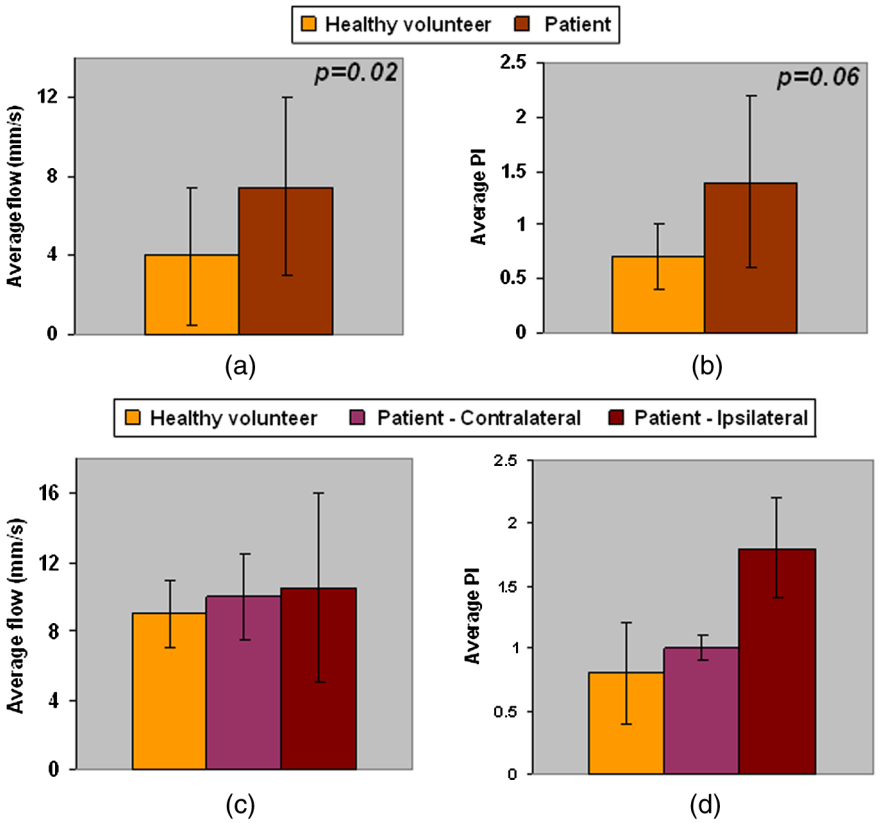

Fig. 4 Results of DOCT image quantification on images from a typical radiation toxicity patient and a healthy volunteer. (a) The average blood velocity in detected vessels of diameter <50 μm, located throughout various regions of the oral cavity, averaged over 20 vessels in the patient and 10 in the healthy volunteer. (b) The average PI for same conditions as (a), averaged over six vessels in the patient and the healthy volunteer. (c) The average blood velocity in detected vessels of diameter <50 μm in the soft palate of a healthy volunteer, and the contralateral (received lower radiation dose) and ipsilateral (received a higher radiation dose) sides of a patient. (d) The average PI for same cases as (c). The error bars show the variance of velocity or PI among the different vessels of the same participant. The total number of the vessels used for calculation in the three subgroups (healthy volunteer, patient contralateral, and patient ipsilateral) in (c) was 3, 5, and 5; and was 2, 3, and 2 in (d).

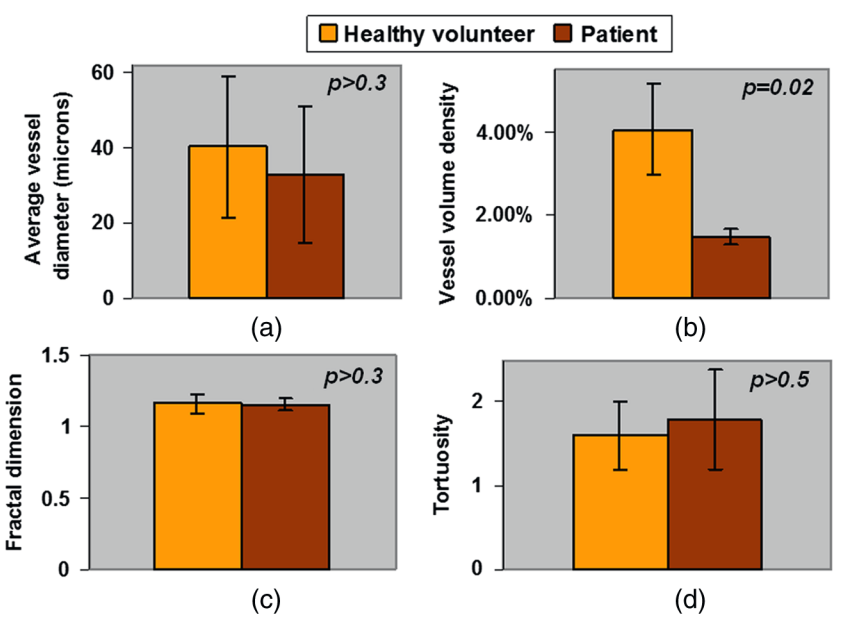

Fig. 5 Results of svOCT image quantification on images from the labial tissue of a typical radiation toxicity patient and a healthy volunteer. (a) Average vessel diameter from 3-D svOCT images, (b) volume density of the vessels, (c) fractal dimension (FD) of the microvascular trees, and (d) average tortuosity values. Error bars in (a) and (d) demonstrate the variability within different vessels of the same participant and the error bars in (b) and (c) represent the changes within the four volume calculations within the 3-D field of view (see Sec. 2.4).

microvasculature, both preclinically (in experimental animals) and clinically in humans.[1,8,11] However, many medical OCT studies to date, if detecting tissue microvasculature at all, have been limited to image visualization without much quantification. Yet vascular image analysis, quantifiable metric development, and validation are needed for more robust understanding and control of diseases and treatments with significant microvascular involvement. This study aimed to address this need by developing a platform for DOCT and svOCT imaging and quantification, in the challenging milieu of a human patient study of late oral radiation toxicity. The late radiation toxicity scenario is clinically motivated by the importance of the problem and the scarcity of currently available objective subsurface assessment and quantification tools, and by recent suggestions that changes in blood flow properties and vessel morphology are implicated in progression of complications.[31] Therefore, in this study, we used the developed DOCT and svOCT microvascular quantification metrics to highlight the differences between the images from one patient and one healthy volunteer in our ongoing clinical study of late oral radiation toxicity.

The DOCT and svOCT imaging and quantification methodology, summarized in Figs. 2 and 3, performed successfully for their intended purpose of human oral microvascular image quantification (Figs. 4 and 5). Various microvascular quantification metrics from DOCT and svOCT were derived and compared between healthy oral tissues and irradiated ones with different radiation doses (Figs. 4 and 5). When technical feasibility is demonstrated, subject to ongoing technological improvements as discussed in particular for DOCT data, no biological or physiological conclusions can be drawn at this stage. Initial findings need to be verified and validated in larger patient and healthy volunteer data sets, which we intend to do as our clinical study continues and draws to a conclusion. Nevertheless, the reported results are suggestive and will inform our future data analysis [e.g., seemingly significant differences in average blood velocity and 3-D microvascular volume density, Fig. 4(a) and 5(b)]. Conversely, some unexpected results, such as similarity of FD and tortuosity in healthy and pathological tissues [Fig. 5(c) and 5(d)], suggest that irradiation may have a modulating effect on the microvasculature. However, we emphasize that these are preliminary conjectures at best, to be more thoroughly pursued as technology evolves, patient numbers accrue, and our radiobiological understanding improves in the process of the ongoing clinical study. We envision that the demonstrated feasibility of the OCT imaging and microvascular quantification platform can help in radiation oncology and in other medical specialties for assessment and monitoring of diseases and treatments with significant microvascular involvement.

5 Conclusion

A novel platform for acquisition and quantification of DOCT and svOCT vascular images was developed and used in an *in vivo* human imaging study on late oral radiation toxicity patients. The methodology aimed to extract blood flow-related parameters (such as average velocity and PI) from the DOCT images, and vessel morphology-related parameters (such as average vessel diameter, vascular volume density, FD, and tortuosity) from the svOCT images, to serve as a quantitative tool for comparing healthy and irradiated oral tissues. Analyzing the calculated values of these parameters for several DOCT and svOCT images of one patient and one healthy volunteer revealed some differences (and some similarities) between the cohorts. The robustness of these initial findings and their radiobiological significance cannot be judged at present and will be thoroughly addressed in the context of our ongoing clinical study. The demonstrated technical feasibility and initial microvascular quantification results are nevertheless encouraging and pave the way for our research on monitoring late oral radiation toxicity using OCT.

References

1. W. Drexler and J. G. Fujimoto, *Optical Coherence Tomography: Technology and Applications*, Springer, Berlin (2008).
2. D. Huang et al., "Optical coherence tomography," *Science* **254**(5035), 1178–1181 (1991).
3. M. E. Brezinski, *Optical Coherence Tomography: Principles and Applications*, Elsevier Inc., London (2006).
4. W. Drexler, "Ultrahigh-resolution optical coherence tomography," *J. Biomed. Opt.* **9**(1), 47–74 (2004).
5. A. M. Zysk et al., "Optical coherence tomography: a review of clinical development from bench to bedside," *J. Biomed. Opt.* **12**(5), 051403 (2007).
6. A. F. Fercher, "Optical coherence tomography—development, principles, applications," *Z. Med. Phys.* **20**(4), 251–276 (2010).
7. L. An, J. Qin, and R. K. Wang, "Ultrahigh sensitive optical microangiography for *in vivo* imaging of microcirculations within human skin tissue beds," *Opt. Express* **18**(8), 8220–8228 (2010).
8. V. X. D. Yang et al., "Endoscopic Doppler optical coherence tomography in the human GI tract: initial experience," *Gastrointest. Endosc.* **61**(7), 879–890 (2005).
9. V. X. D. Yang et al., "High speed, wide velocity dynamic range Doppler optical coherence tomography (Part I): system design, signal processing, and performance," *Opt. Express* **11**(7), 794–809 (2003).
10. V. X. D. Yang and I. A. Vitkin, "Principles of Doppler OCT," Chapter 32 in *Optical Coherence Tomography in Cardiovascular Research*, E. Regar, T. G. van Leeuwen, and P. W. Serruys, Eds., pp. 305–318, Informa Healthcare, United Kingdom (2007).
11. A. Mariampillai et al., "Optimized speckle variance OCT imaging of microvasculature," *Opt. Lett.* **35**(8), 1257–1259 (2010).
12. "ClinicalTrials.gov," http://www.clinicaltrials.gov/ (5 October 2012).
13. L. F. Fajardo, L-G. M. Berthrong, and R. E. Anderson, *Radiation Pathology*, Oxford University Press Inc., New York (2001).
14. J. W. Eveson and C. Scully, *Color Atlas of Oral Pathology*, Mosby-Wolfe, London, United Kingdom (1995).
15. F. Denis et al., "Late toxicity results of the GORTEC 94–01 randomized trial comparing radiotherapy with concomitant radiochemotherapy for advanced-stage oropharynx carcinoma: comparison of LENT/SOMA, RTOG/EORTC, and NCI-CTC scoring systems," *Int. J. Radiat. Oncol. Biol. Phys.* **55**(1), 93–98 (2003).
16. D. G. Baker and R. J. Krochak, "The response of the microvascular system to radiation: a review," *Cancer Invest.* **7**(3), 287–294 (1989).
17. B. Davoudi et al., "Noninvasive *in vivo* structural and vascular imaging of human oral tissues with spectral domain optical coherence tomography," *Biomed. Opt. Express* **3**(5), 826–839 (2012).
18. "WMA Declaration of Helsinki—Ethical Principles for Medical Research Involving Human Subjects," http://www.wma.net/en/30publications/10policies/b3/ (5 October 2012).
19. M. Aleksic et al., "Pulsatility index determination by flowmeter measurement: a new indicator for vascular resistance?" *Eur. Surg. Res.* **36**(6), 345–349 (2004).
20. L. Conroy, R. S. DaCosta, and I. A. Vitkin, "Quantifying tissue microvasculature with speckle variance optical coherence tomography," *Opt. Lett.* **37**(15), 3180–3182 (2012).
21. C. A. Schneider, W. S. Rasband, and K. W. Eliceiri, "NIH Image to Image J: 25 years of image analysis," *Nat. Methods* **9**(7), 671–675 (2012).
22. M. H. Longair, D. A. Baker, and J. D. Armstrong, "Simple Neurite Tracer: Open Source software for reconstruction, visualization and analysis of neuronal processes," *Bioinformatics* **27**(17), 1–2 (2011).
23. B. Lemasson et al., "*In vivo* imaging of vessel diameter, size, and density: a comparative study between MRI and histology," *Magn. Reson. Med.* **69**(1), 1–9 (2012).

24. T. L. Jackson, *Modeling Tumor Vasculature: Molecular, Cellular, and Tissue Level Aspects and Implications*, Springer, New York (2012).
25. P.-M. Robitaille and L. J. Berliner, *Ultra High Field Magnetic Resonance Imaging*, Springer Science, New York (2006).
26. J. Baish and R. Jain, "Fractals and Cancer," *Cancer Res.* **60**(14), 3683–3688 (2000).
27. R. Karshafian, P. N. Burns, and M. R. Henkelman, "Transit time kinetics in ordered and disordered vascular trees," *Phys. Med. Biol.* **48**(19), 3225–3237 (2003).
28. A. Karperien, "FracLac for Image J, version 2.5," http://rsb.info.nih.gov/ij/plugins/fraclac/FLHelp/Introduction.htm (1999–2012).
29. E. Bullitt et al., "Measuring tortuosity of the intracerebral vasculature from MRA images," *IEEE Trans. Med. Imag.* **22**(9), 1163–1171 (2003).
30. G. V. Belle et al., *Biostatistics: A Methodology for the Health Sciences, Wiley Series in Probability and Statistics*, Wiley, Hoboken (2004).
31. S. Hamilton et al., "Microvascular changes in radiation-induced oral mucositis," *J. Otolaryngol. Head Neck Surg.* **37**(5), 730–737 (2008).